Light emission polarization properties of semipolar InGaN/GaN quantum well

Hung-Hsun Huang and Yuh-Renn Wu[a)]
Department of Electrical Engineering and Graduate Institute of Photonics and Optoelectronics, National Taiwan University, Taipei 10617, Taiwan

(Received 17 November 2009; accepted 25 January 2010; published online 11 March 2010)

As many reports show that the InGaN quantum wells grown on semipolar substrate have better efficiency in the green spectrum, it is important to understand the light emission properties of these semipolar quantum wells. In this paper, we have studied the optical characteristics of a semipolar InGaN/GaN quantum well with different growth orientations. Also, the most common growth directions such as $(10\bar{1}\bar{3})$ and $(11\bar{2}2)$ planes are studied in details. The self-consistent Poisson and 6×6 $k\cdot p$ Schrödinger solver has been applied to study the band structure of the semipolar InGaN-based quantum well. We find that the light emission polarization ratio has a very interesting switching behavior under different conditions of indium compositions, quantum well widths, and injection carrier densities. Our results show that the semipolar InGaN quantum well has a potential to be a polarized light source under certain conditions. © *2010 American Institute of Physics*. [doi:10.1063/1.3327794]

I. INTRODUCTION

In recent years, InGaN/GaN quantum wells have been widely used in several areas such as liquid crystal display (LCD) backlight module, blue-ray laser diode (LD), and solid state lighting. However, due to the strong polarization field caused by the strained InGaN layer in the *c*-plane, the quantum-confined Stark effect (QCSE) is induced and the internal quantum efficiency is reduced. The alloying of high indium composition in InGaN-based quantum well structure will not only lead to the higher lattice mismatch but also influence the growth quality of the material. As a result, there exists a "green-yellow gap"[1] in light emitting diodes (LEDs).

To reduce the internal electric field in the quantum well, one is to grow the InGaN quantum well along the $(11\bar{2}0)$ direction (*a*-plane)[2–4] or along the $(1\bar{1}00)$ direction (*m*-plane),[5–7] where the polarization charge is not formed at the interface or along some semipolar planes such as $(11\bar{2}2)$ direction,[8–11] $(10\bar{1}\bar{3})$ direction,[12,13] and $(1\bar{1}01)$ direction.[14] Figures 1(a)–1(c) show the schematics of several common semipolar planes. The advantages of using nonpolar or semipolar LEDs are not only reducing the QCSE but also making a polarized light source, which is important in applications needing a polarized light source, such as LD and LCD backlight module.[15,16]

The indium incorporation of the nonpolar InGaN/GaN quantum well is lower than that of the conventional *c*-plane InGaN-based quantum well. However, the indium incorporation of the semipolar quantum well may be comparable to, or greater than that of the *c*-plane one. Therefore, it is possible to overcome the green-yellow gap with semipolar InGaN quantum wells. It means that the semipolar device has a great chance to replace the nonpolar device in the longer wavelength such as green and yellow light emitters due to the higher indium incorporation.[1,11,17,18]

There have been some studies of semipolar InGaN/GaN quantum well LEDs with different growth orientations.[12,19–27] They observed an in-plane anisotropic polarization feature of the semipolar quantum well, as well as the nonpolar one. The optical polarization properties of semipolar quantum well will be affected by the anisotropic normal strain and the shear strain components. As we know, the variation in the quantum confinement effect for the semipolar quantum well depends on the out-plane effective mass. Therefore, the analysis of optical polarization properties in semipolar orientation is more complicated than that in the

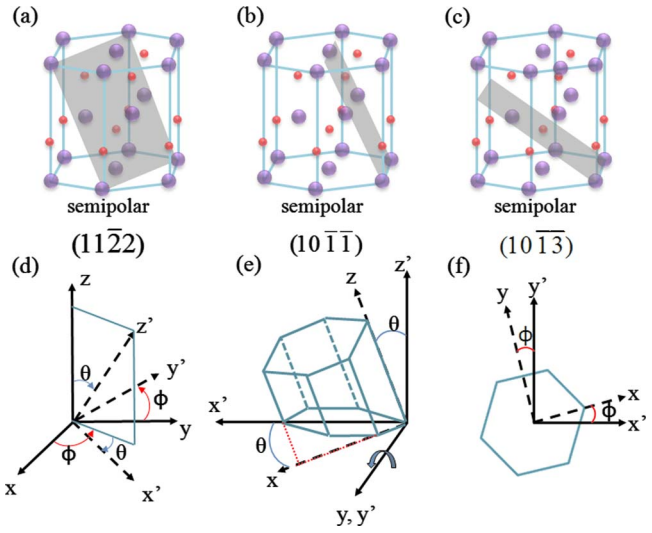

FIG. 1. (Color online) [(a)–(c)] are semipolar planes $(11\bar{2}2)$, $(10\bar{1}\bar{1})$, and $(10\bar{1}\bar{3})$, respectively. (d) is the configuration of the rotating coordinate system from (x,y,z) to (x',y',z'); [(e) and (f)] are the schematic illustrations of rotating GaN crystal structure with θ angle and ϕ angle, respectively.

[a)]Electronic addresses: yrwu@cc.ee.ntu.edu.tw and yrwu@ntu.edu.tw.

nonpolar orientation. Also, the injected carrier density plays an important role in determining the light emission property. Usually with higher carrier injection density, more subbands are filled and it modifies the polarization ratio of light.

In this work, we work on the calculation of the optical polarization properties of InGaN semipolar quantum wells with different growth orientations. We applied a self-consistent Poisson and 6×6 $k\cdot p$ Schrödinger method[28,29] to obtain the band bending caused by piezoelectric polarization, the band structure, energy subband levels, and wave functions. The strain deformation effect is considered here. The semipolar plane $(10\bar{1}\bar{3})$ and $(11\bar{2}\bar{2})$ will be discussed in great detail. The result of $(10\bar{1}\bar{1})$ is close to $(11\bar{2}\bar{2})$ so that $(11\bar{2}\bar{2})$ can be taken as a reference.

II. FORMALISM

To understand the light emission polarization property of the semipolar quantum well system, we need to address the following issues: (1) the valence band states mixing, (2) the energy separation of CH1 and CH2 bands, and (3) the effective mass ratio of CH1 to CH2 band which strongly affects the ability of the quantum confinement. We applied 6×6 $k\cdot p$ method[30] for calculating the valence band and effective mass approximation method for calculating the conduction band. The 6×6 Hamiltonian of $k\cdot p$ model can be expressed as

$$H^v=\begin{pmatrix} F & 0 & -H^* & 0 & K^* & 0 \\ 0 & G & \Delta & -H^* & 0 & K^* \\ -H & \Delta & \lambda & 0 & I^* & 0 \\ 0 & -H & 0 & \lambda & \Delta & I^* \\ K & 0 & I & \Delta & G & 0 \\ 0 & K & 0 & I & 0 & F \end{pmatrix}\begin{matrix} |u_1\rangle \\ |u_2\rangle \\ |u_3\rangle \\ |u_4\rangle \\ |u_5\rangle \\ |u_6\rangle \end{matrix}, \tag{1}$$

where

$$F=\Delta_1+\Delta_2+\lambda+\theta,\quad G=\Delta_1-\Delta_2+\lambda+\theta,$$

$$\lambda=\frac{\hbar^2}{2m_0}[A_1k_z^2+A_2(k_x^2+k_y^2)]+D_1\epsilon_{zz}+D_2(\epsilon_{xx}+\epsilon_{yy}),$$

$$\theta=\frac{\hbar^2}{2m_0}[A_3k_z^2+A_4(k_x^2+k_y^2)]+D_3\epsilon_{zz}+D_4(\epsilon_{xx}+\epsilon_{yy}),$$

$$K=\frac{\hbar^2}{2m_0}A_5(k_x+ik_y)^2+D_5(\epsilon_{xx}-\epsilon_{yy}+2i\epsilon_{xy}),$$

$$H=\frac{\hbar^2}{2m_0}i[A_6k_z(k_x+ik_y)+A_7(k_x+ik_y)]+iD_6(\epsilon_{xz}+i\epsilon_{yz}),$$

$$I=\frac{\hbar^2}{2m_0}i[A_6k_z(k_x+ik_y)-A_7(k_x+ik_y)]+iD_6(\epsilon_{xz}+i\epsilon_{yz}),$$

$$\Delta=\sqrt{2}\Delta_3. \tag{2}$$

D_1-D_6 are the deformation potentials and A_1-A_7 are the fitting parameters to valence band structures. k_i and ϵ_{ij} $(i,j=x,y,z)$ are the wave vector and the strain tensor. Δ_1 is the crystal-field energy. Δ_2 and Δ_3 are the spin-orbit energy parameters. $|u_1\rangle-|u_6\rangle$ are the bases of the Hamiltonian, which are $1/\sqrt{2}|X+iY,\uparrow\rangle$, $1/\sqrt{2}|X+iY,\downarrow\rangle$, $|Z,\uparrow\rangle$, $|Z,\downarrow\rangle$, $1/\sqrt{2}|X-iY,\uparrow\rangle$, and $1/\sqrt{2}|X-iY,\downarrow\rangle$, respectively. The polarization of the emission light is strongly affected by these bases. The parameters we used for this simulation can be found in Ref. 4. If we consider the arbitrary crystal growth orientation, the Hamiltonian, strain tensor, and piezoelectric effect can be obtained by using a rotation matrix

$$U=\begin{pmatrix} \cos\theta\cos\phi & \cos\theta\sin\phi & -\sin\theta \\ -\sin\phi & \cos\phi & 0 \\ \sin\theta\cos\phi & \sin\theta\sin\phi & \cos\theta \end{pmatrix}, \tag{3}$$

where the angles θ and ϕ denote the rotation angle from the z-axis (c-axis) to the x-axis and from x-axis to y-axis, respectively. We rotate the crystal growth axis (defined as the z'-axis) from (x,y,z) coordinate to (x',y',z') coordinate, as shown in Figs. 1(d)–1(f). The relations between the original coordinate system and the rotated coordinate systems for the wave vectors, strain tensors, and elastic stiffness constants are expressed as

$$k_i'=\sum_\alpha U_{i\alpha}k_\alpha, \tag{4}$$

$$\epsilon_{ij}'=\sum_{\alpha\beta}U_{i\alpha}U_{j\beta}\epsilon_{\alpha\beta}, \tag{5}$$

$$C_{ijkl}'=\sum_{\alpha\beta\gamma\delta}U_{i\alpha}U_{j\beta}U_{k\gamma}U_{l\delta}C_{\alpha\beta\gamma\delta}. \tag{6}$$

From Eq. (6), we can obtain the rotated elastic stiffness constants, which are defined through Hooke's Law. The parameters of elastic stiffness constants we used are also listed in Ref. 4. For the Hamiltonian of the crystal growth orientation z'-axis, the k_z' will be transformed into the differential form $-i\partial/\partial z'$.

We apply the self-consistent Poisson and 6×6 $k\cdot p$ Schrödinger solver to iteratively solve the band structure, energy levels, and wave functions of electron and hole until they are converged. From the basis of the Hamiltonian, we can obtain the polarization-dependent optical matrix element. The x, y, and z polarized light is then transformed into x', y', and z' coordinate to present the in-plane and out-plane polarized light. The light emission rate is calculated by

$$R_{sp}=\int d(\hbar\omega)\frac{e^2n_r\hbar\omega}{m_0^2\varepsilon_0c^3\hbar^2}\sum_{i,j}\int\frac{2}{(2\pi)^2}d^2\vec{k}|\hat{a}\cdot\vec{p}_{i,j}|^2 \times\frac{1}{\sigma\sqrt{2\pi}}\exp\left[\frac{-(E_{i,j}-\hbar\omega)^2}{2\sigma^2}\right]f^e[E_i^e(\vec{k})]f^h[E_j^h(\vec{k})] \quad (\mathrm{cm^{-2}\,eV^{-1}\,s^{-1}}), \tag{7}$$

where f^e and f^h are Fermi–Dirac function, n_r is the refractive index, and $E_{i,j}$ is the effective bandgap between states i and j. σ is the inhomogeneous broadening factor.

In order to analyze the polarization, we need to define the polarization ratio. Considering the different measured orientations, we define the polarization ratios as

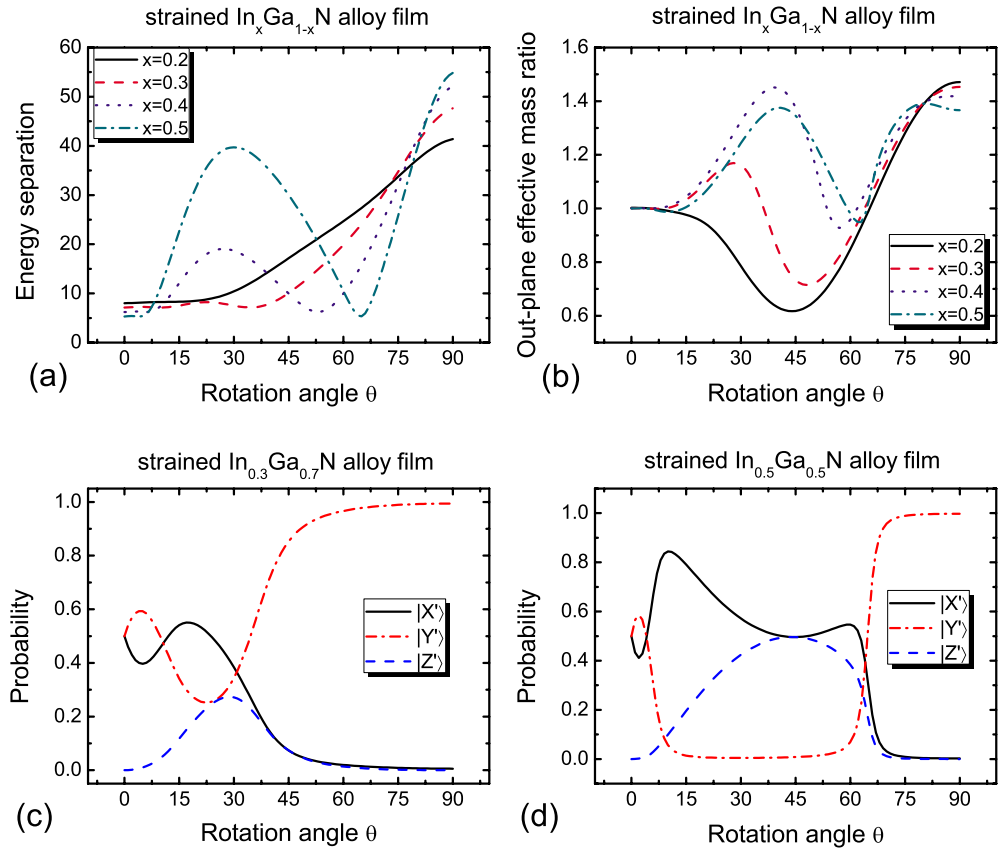

FIG. 2. (Color online) (a) The energy separation of CH1–CH2 band as a function of rotation angle for the strained InGaN layer. (b) The out-plane effective mass ratio of CH1 to CH2 band as a function of rotation angle for the strained InGaN layer. [(c) and (d)] are the $|X'\rangle$, $|Y'\rangle$, and $|Z'\rangle$ state probabilities of CH1 band as a function of rotation angle for the strained $In_{0.3}Ga_{0.7}N$ layer and $In_{0.5}Ga_{0.5}N$ layer, respectively.

$$\rho_{y'x'} = \frac{I_{y'} - I_{x'}}{I_{y'} + I_{x'}},$$

$$\rho_{y'z'} = \frac{I_{y'} - I_{z'}}{I_{y'} + I_{z'}},$$

$$\rho_{y'(x'+z')} = \frac{I_{y'} - I_{(x'+z')}}{I_{y'} + I_{(x'+z')}}, \tag{8}$$

where $I_{x'}$, $I_{y'}$, and $I_{z'}$ are the emission intensity with the light polarization parallel to the x'-axis, y'-axis, and z'-axis, respectively. Also, $I_{(x'+z')}$ represents the summation of $I_{x'}$ and $I_{z'}$.

III. RESULTS

Our previous studies on the *a*-plane InGaN quantum well[4] have shown that increasing strain and making the effective mass difference large are the key points to enhance the polarization ratio of the emitted light. To achieve the larger polarization ratio, the topmost subband state is suggested to be purely $|X'\rangle$-like, $|Y'\rangle$-like, or $|Z'\rangle$-like state for surface emitting. Also, the energy separation of the first band to the second band should be large. Hence, the strain induced energy separation should be strong. For a strong quantum confinement effect when making quantum wells, a larger out-plane effective mass difference between the first and the second subbands is needed.

Figures 2(a) and 2(b) show the changes of the out-plane effective mass ratio and the energy separation of CH1–CH2 bands with different crystal growth orientations for biaxial strained InGaN alloy films. We can find that the larger effective mass ratio is located at $\theta = 75° - 90°$. Moreover, for higher indium composition, another peak is near 30°–40°. For the θ near 75°–90°, the CH1 band is dominated by the $|Y'\rangle$-liked state, as shown in Figs. 2(c) and 2(d). On the other hand, the peaks near 30°–40° is dominated by $|X'\rangle$- and $|Z'\rangle$-liked states, where the two states are not completely separated.

As shown in Figs. 2(a) and 2(b), we can find that the energy separation trend and out-plane effective mass difference change significantly at $\theta = 15° - 60°$ for different indium composition cases. As we know, the shear strain is no longer 0 for the semipolar plane. Therefore, the deformation term D_6 starts to play an important role here. The shear strain will lift up the $|X'\rangle$ and $|Z'\rangle$ states, while the normal strain will lift up the $|Y'\rangle$ state. It means that the two kinds of strain effects compete with each other and results in the switching of the energy band positions. If we compared the 30% InGaN to 50% InGaN from $\theta = 13°$ to 52°, we can find that the energy separation of the first state to the second state becomes larger due to the stronger influence of the shear strain. A switching behavior is observed for indium composition

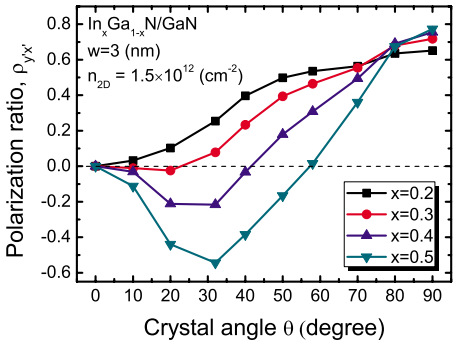

FIG. 3. (Color online) The polarization ratio ($|Y'\rangle$ to $|X'\rangle$) of light emitted from an $In_xGa_{1-x}N/GaN$ quantum well as a function of crystal angle. The well width is 3 nm and injection carrier density is 1.5×10^{12} cm^{-2}.

larger than 40%. From Fig. 2, we can find that the better polarization ratio can be achieved at θ around 15°–30° and 75°–90°.

In the previous case, we show the result for a bulk strained InGaN alloy film, where the quantum confinement effect is not considered. Here, we further include the quantum confinement effect in a strained InGaN quantum well. Figure 3 shows the polarization ratio of an InGaN/GaN quantum well as a function of crystal angle for different indium compositions. Similar to the strained bulk InGaN alloy film, the InGaN-based quantum well system with growth orientation along θ=75°–90° has higher polarization ratio. However, due to the limit of the growth technique, it is not possible for all arbitrary growth orientation. Moreover, the most common semipolar planes mentioned earlier are along $(11\bar{2}2)$ and $(10\bar{1}3)$ directions, which is rotated 58° and 32° from *c*-axis, respectively. Therefore, we will study in detail for the light emission polarization properties of $(11\bar{2}2)$ and $(10\bar{1}3)$ semipolar InGaN/GaN quantum wells.

A. Semipolar $(10\bar{1}3)$ InGaN quantum well

Figure 4 shows the valence band structure of the InGaN-based semipolar $(10\bar{1}3)$ quantum well with indium composition equal to 20%. As mentioned in the strained bulk case where the first band is mainly $|Y'\rangle$ state, the $|Y'\rangle$ state is pulled down to be the second subband by the quantum con-

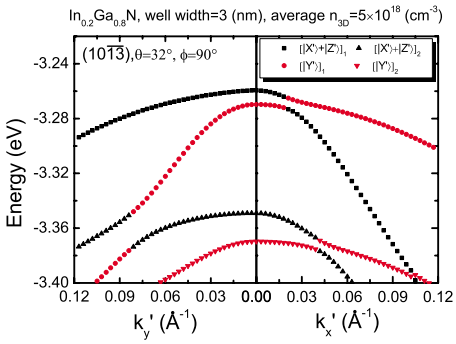

FIG. 4. (Color online) The valence band dispersion relation of the $(10\bar{1}3)$ (intersects the *c*-plane at 32°) semipolar $In_{0.2}Ga_{0.8}N/GaN$ quantum well.

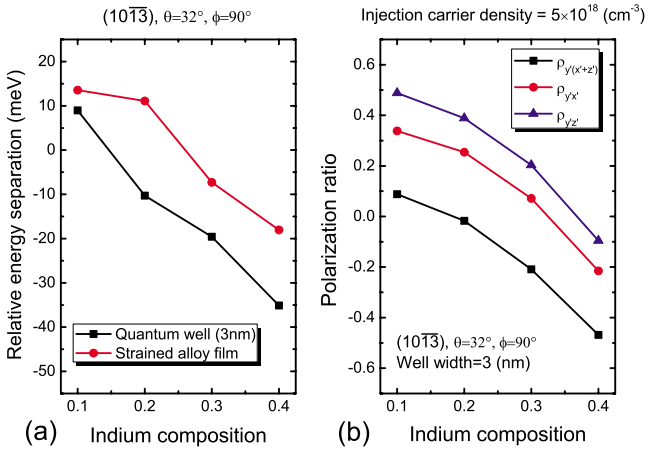

FIG. 5. (Color online) (a) The relative energy separation of the $(10\bar{1}3)$ InGaN/GaN quantum well structure and the strained InGaN alloy film as a function of indium composition, respectively. Note that the relative energy separation is defined as the difference from the $|Y'\rangle$ subband to the $|X'\rangle+|Z'\rangle$ subband. (b) The polarization ratios of the InGaN/GaN $(10\bar{1}3)$ quantum well as a function of indium composition.

finement effect when the quantum well is formed. It is due to that the out-plane effective mass of the $|Y'\rangle$ state is smaller than that of the $0.6|X'\rangle+0.4|Z'\rangle$ state.

Figures 5(a) and 5(b) show the relative energy separation of the $|Y'\rangle$ subband to the $|X'\rangle+|Z'\rangle$ subband and the polarization ratios of InGaN/GaN $(10\bar{1}3)$ semipolar quantum well as a function of indium composition, respectively. Note that the relative energy separation is defined as the difference from the $|Y'\rangle$ subband to the $|X'\rangle+|Z'\rangle$ subband. It means that if the $|X'\rangle+|Z'\rangle$ subband state is the topmost state, the relative energy separation would be a negative value. From Fig. 5(a), we can find that the $|X'\rangle+|Z'\rangle$ subband will be the topmost subband with higher indium composition. Therefore, the polarization ratio decreases as the indium composition increases. We can find that $|X'\rangle+|Z'\rangle$ state becomes the first subband when the indium composition is larger than 10%. However, if we simply compare the polarization ratio for the y'-polarized light to the x'-polarized light, the switching is happened when the indium composition is larger than 30%. This is due to the mixing of $|X'\rangle$ and $|Z'\rangle$ states so that carriers filled in the first subband do not emit pure x'-polarized light.

Figures 6(a) and 6(b) show the relative energy separation and the polarization ratio as a function of well width for different indium compositions, respectively. Since the effective mass of the confined direction of the $|X'\rangle+|Z'\rangle$ subband is larger than that of the $|Y'\rangle$ subband, the quantum confinement effect becomes weaker when the well width increases.

Hence, the absolute value of the relative energy separation decreases as the well width increases and resulted in the increase in the y'-polarization component. Therefore, the polarization ratio increases as the well width increases.

Figure 7 shows the change in polarization ratio $\rho_{y'x'}$, versus injection carrier density of the $(10\bar{1}3)$ InGaN quantum well. The band bending caused by the polarization charge decreases as the injection carrier density increases due to the screening effect. Also, when more carriers are injected into

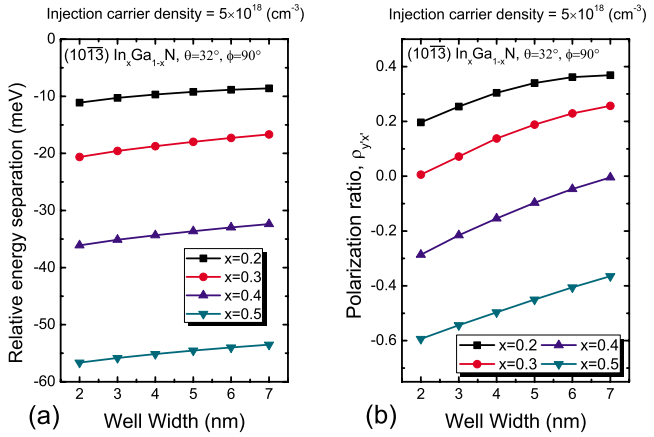

FIG. 6. (Color online) (a) The relative energy separation of the $(10\bar{1}3)$ InGaN/GaN quantum well structure as a function of well width for different indium compositions. Note that the relative energy separation is defined as the difference from the $|Y'\rangle$ subband to the $|X'\rangle+|Z'\rangle$ subband. (b) The polarization ratio of the InGaN/GaN $(10\bar{1}3)$ quantum well as a function of well width for different indium compositions.

the quantum well, the higher energy states are filled with carriers. As a result, there are more carriers being filled in $|Y'\rangle$-like state under the high injection condition compared with the low injection condition. The y'-polarized light component increases as the carrier injection density increases. Therefore, the absolute value of polarization ratio increases under high carrier injection condition. The simulation result shows that if we want to design a cavity for the laser diode, for lower indium composition, we should consider to excite the y'-polarized light. Especially when carrier injection increases, y'-polarized light will be enhanced. However, for 40%–50% indium cases, x'-polarized light is dominated and the increase in injection carriers will make the polarization ratio worse.

B. Semipolar $(11\bar{2}2)$ InGaN quantum well

Semipolar $(11\bar{2}2)$ InGaN quantum well has attracted a great attention for green light emitters.[31,32] There are some studies indicating that the indium incorporation of the $(11\bar{2}2)$ InGaN-based quantum well is similar to or even greater than that of the c-plane one.[33] As a result, there is a strong potential in the $(11\bar{2}2)$ semipolar LEDs for long wavelength light emitter application such as green and yellow LEDs.[24] Figures 8(a) and 8(b) show the valence band structure of the InGaN-based semipolar $(11\bar{2}2)$ quantum well with indium composition equal to 20% and 50%, respectively. We can find that the subband mixed with $|X'\rangle$-like and $|Z'\rangle$-like states becomes the topmost band for the 50% indium case. Moreover, for 20% indium case, the state is purely dominated by $|Y'\rangle$-like state. It is due to that the contribution of the shear strain effect becomes significant in the high indium composition case. Therefore, the switching phenomenon occurs in the indium composition near 40%–50%. It means that the $|X'\rangle+|Z'\rangle$ subband is lifted up to be the topmost subband, which is also reported in Ref. 25.

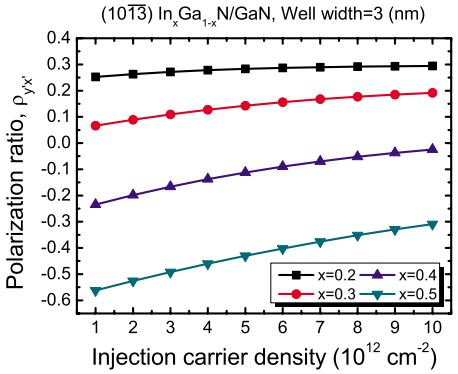

FIG. 7. (Color online) The shift in the polarization ratio $\rho_{y'x'}$ vs the injection carrier density of the semipolar $(10\bar{1}3)$ quantum well for different indium compositions.

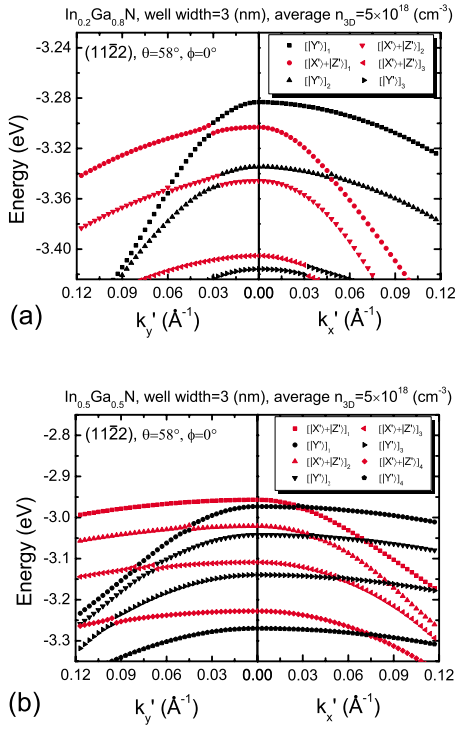

FIG. 8. (Color online) The valence band dispersion relation of the $(11\bar{2}2)$ (intersects the c-plane at 58°) semipolar $In_xGa_{1-x}N/GaN$ quantum well. (a) $x=0.2$ and (b) $x=0.5$.

Figures 9(a) and 9(b) show the relative energy separation of the $|Y'\rangle$ subband to the $|X'\rangle+|Z'\rangle$ subband and the polarization ratios of the InGaN/GaN $(11\bar{2}2)$ semipolar quantum well as a function of the indium composition, respectively. Because the shear strain ϵ_{xz} becomes dominant as the indium composition increases, the relative energy separation decreases as the indium composition increases. It is worth noting that the relative energy separation of the 20% indium composition is slightly larger than that of the 10% indium composition because the crystal-field energy Δ_1 of InN is larger than that of GaN. In addition, the relative energy separation in the quantum well is similar to that of the strained alloy film since the effective mass difference of the two subband states is small. As shown in Fig. 9(b), we can find that the polarization ratios decrease as the indium composition increases because the x'-polarized and z'-polarized components become stronger. As shown in Fig. 9(a), there is a

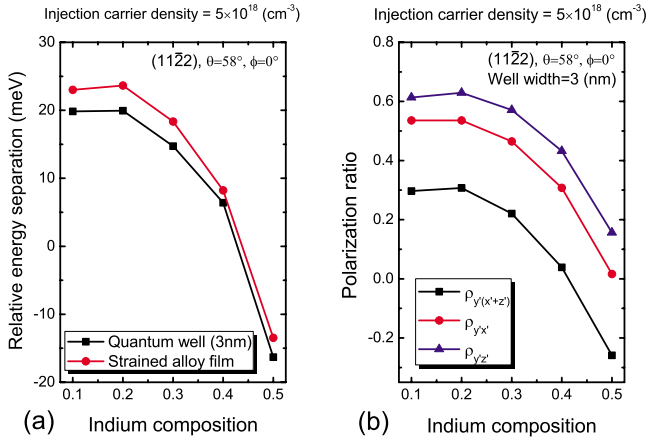

FIG. 9. (Color online) (a) The relative energy separation of the (11$\bar{2}$2) InGaN/GaN quantum well structure and the strained InGaN alloy film as a function of indium composition, respectively. Note that the relative energy separation is defined as the difference from the $|Y'\rangle$ subband to the $|X'\rangle + |Z'\rangle$ subband. (b) The polarization ratios of the InGaN/GaN (11$\bar{2}$2) quantum well as a function of indium composition.

switch between $|Y'\rangle$-like state and ($|X'\rangle+|Z'\rangle$)-like state near 40% indium composition. It has shown a good agreement with some published experimental works,[25,31] which the polarization switching is observed around 30% indium composition.

Figures 10(a) and 10(b) show the relative energy separation and the polarization ratio as a function of well width for different indium compositions, respectively. As mentioned earlier, the effective mass of the $|X'\rangle+|Z'\rangle$ subband is slightly larger than that of the $|Y'\rangle$ subband. Therefore, for indium composition smaller than 40% where the $|Y'\rangle$-liked is the first subband, the smaller quantum well width will make the two subbands closer. When the indium composition is larger than 40%, $|Y'\rangle$-liked subband becomes the second subband and smaller quantum well width will make the separation of two subbands larger. As we know, since the QCSE is

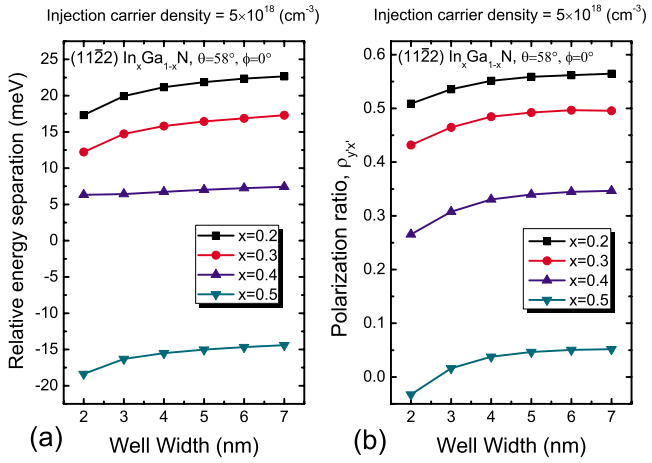

FIG. 10. (Color online) (a) The relative energy separation of the (11$\bar{2}$2) InGaN/GaN quantum well structure as a function of well width for different indium compositions. Note that the relative energy separation is defined as the difference from the $|Y'\rangle$ subband to the $|X'\rangle+|Z'\rangle$ subband. (b) The polarization ratio of the InGaN/GaN (11$\bar{2}$2) quantum well as a function of well width for different indium compositions.

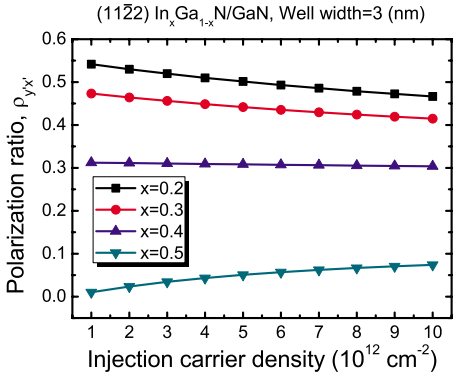

FIG. 11. (Color online) The shift in the polarization ratio $\rho_{y'x'}$ vs the injection carrier density of the semipolar (11$\bar{2}$2) quantum well for different indium compositions.

weaker in the semipolar plane, we can have a large quantum well width, which is good for high power application. Hence, for the indium composition below 40%, it is good to make a wider quantum well for high power applications and also keep good polarization ratio.

Figure 11 shows the change in polarization ratio $\rho_{y'x'}$ versus injection carrier density of the (11$\bar{2}$2) quantum well for different indium compositions. For the indium composition smaller than 40%, the $|X'\rangle+|Z'\rangle$ subband state is the second subband in the system. The x' and z' polarization components are getting stronger when more carriers are injected into the quantum well. Hence, the increase in injection will make the polarization ratio $\rho_{y'x'}$ weaker. However, for the indium composition larger than 40%, the subbands are switched. The $|Y'\rangle$ subband state becomes the second subband and therefore, the increase in injection will make the polarization ratio $\rho_{y'x'}$ stronger.

Note that the deformation potentials of InN are still not determined very well. For example, as shown in Table I, the deformation potentials of InN from Ref. 25 are very different from the values used in Ref. 34. As we know that the values of deformation potential D_5 and D_6 are critical to the polarization behavior. Therefore, it is important to know how these different values influence the simulation result. Figure 12 shows the polarization ratio $\rho_{y'x'}$ versus the indium composition with different values of deformation potentials listed in Table I. We can find that the change in the deformation

TABLE I. Deformation potential parameters of InN.

Deformation potentials (eV)	A	B	C
a_c	−1.4[a]		
D_1	−1.76[a]	2.22[b]	2.22[b]
D_2	3.43[a]	3.2[b]	3.2[b]
D_3	5.19[a]	2.68[b]	0.10[c]
D_4	−2.595[a]	−1.74[b]	−0.05[c]
D_5	−2.33[a]	−2.07[b]	−3.5[c]
D_6	−5.5[d]	−3.96[b]	−8.8[c]

[a]Reference 35.
[b]Reference 34.
[c]Reference 25.
[d]Reference 36.

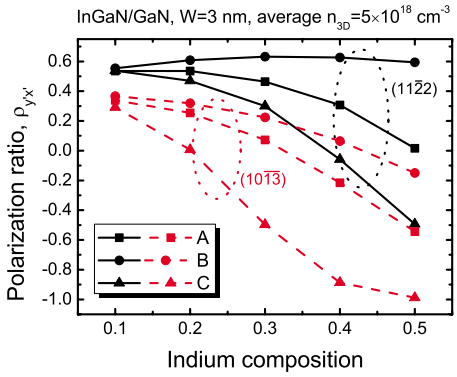

FIG. 12. (Color online) The polarization ratio $\rho_{y'x'}$ of the semipolar $(10\bar{1}3)$ and $(11\bar{2}2)$ InGaN/GaN quantum wells as a function of indium composition with different material parameters listed in Table I.

potential has a significant influence on the polarization ratio, especially for the higher indium composition cases. These changes are mainly from the contribution of the terms $D_5(\epsilon_{xx}-\epsilon_{yy})$ and $D_6(\epsilon_{xz})$ in Eq. (2). If we use the material parameters B listed in Table I,[34] we may not be able to obtain the polarization switching in the $(11\bar{2}2)$ semipolar plane. Moreover, the parameters suggested by Ueda *et al.*[25] show an earlier switching compared with our results. Therefore, it is very important to further determine the material parameter of InN to provide a better prediction in the future.

IV. CONCLUSION

In conclusion, we have done a detail study of the optical anisotropic behavior for the semipolar quantum well with different growth orientations. The more detail studies on the influence of the indium composition, well width, and injection carrier density for the $(10\bar{1}3)$ and $(11\bar{2}2)$ semipolar InGaN/GaN quantum wells are performed in this work. The optical polarization properties are strongly affected by the strain effect and effective mass ratio, especially from the shear strain component. Furthermore, the polarization switching behavior at semipolar plane $(11\bar{2}2)$ has been observed in our calculation, which provides an explanation to the experimental results.[25] Our work provides an useful information for designing the semipolar $(10\bar{1}3)$ and $(11\bar{2}2)$ InGaN quantum well for applications, such as LCD backlight modules and laser diodes.

ACKNOWLEDGMENTS

The authors would like to thank National Science Council in Taiwan for the financial support, under Grant Nos. NSC-97-2221-E002-050 and 98-2221-E-002-037-MY2, and Aim for Top University Project from the Ministry of Education, Taiwan.

[1]M. Crawford, IEEE J. Sel. Top. Quantum Electron. **15**, 1028 (2009).
[2]T. S. Ko, T. C. Lu, T. C. Wang, J. R. Chen, R. C. Gao, M. H. Lo, H. C. Kuo, S. C. Wang, and J. L. Shen, J. Appl. Phys. **104**, 093106 (2008).
[3]C. H. Chiu, S. Y. Kuo, M. H. Lo, C. C. Ke, T. C. Wang, Y. T. Lee, H. C. Kuo, T. C. Lu, and S. C. Wang, J. Appl. Phys. **105**, 063105 (2009).
[4]H.-H. Huang and Y.-R. Wu, J. Appl. Phys. **106**, 023106 (2009).
[5]H. Masui, A. Chakraborty, B. A. Haskell, U. K. Mishra, J. S. Speck, S. Nakamura, and S. P. DenBaars, Jpn. J. Appl. Phys., Part 2 **44**, L1329 (2005).
[6]K.-C. Kim, M. C. Schmidt, H. Sato, F. Wu, N. Fellows, Z. Jia, M. Saito, S. Nakamura, S. P. DenBaars, J. S. Speck, and K. Fujito, Appl. Phys. Lett. **91**, 181120 (2007).
[7]H. Masui, H. Yamada, K. Iso, S. Nakamura, and S. P. DenBaars, J. Phys. D **41**, 225104 (2008).
[8]K. Nishizuka, M. Funato, Y. Kawakami, S. Fujita, Y. Narukawa, and T. Mukai, Appl. Phys. Lett. **85**, 3122 (2004).
[9]M. Funato, M. Ueda, Y. Kawakami, Y. Narukawa, T. Kosugi, M. Takahashi, and T. Mukai, Jpn. J. Appl. Phys., Part 2 **45**, L659 (2006).
[10]H. Masui, T. J. Baker, M. Iza, H. Zhong, S. Nakamura, and S. P. DenBaars, J. Appl. Phys. **100**, 113109 (2006).
[11]N. Fellows, H. Sato, H. Masui, S. P. DenBaars, and S. Nakamura, Jpn. J. Appl. Phys. **47**, 7854 (2008).
[12]R. Sharma, P. M. Pattison, H. Masui, R. M. Farrell, T. J. Baker, B. A. Haskell, F. Wu, S. P. DenBaars, J. S. Speck, and S. Nakamura, Appl. Phys. Lett. **87**, 231110 (2005).
[13]A. Chakraborty, T. J. Baker, B. A. Haskell, F. Wu, J. S. Speck, S. P. Denbaars, S. Nakamura, and U. K. Mishra, Jpn. J. Appl. Phys., Part 2 **44**, L945 (2005).
[14]M. Feneberg, F. Lipski, R. Sauer, K. Thonke, P. Bruckner, B. Neubert, T. Wunderer, and F. Scholz, J. Appl. Phys. **101**, 053530 (2007).
[15]M. Kubota, K. Okamoto, T. Tanaka, and H. Ohta, Appl. Phys. Lett. **92**, 011920 (2008).
[16]H. Masui, H. Yamada, K. Iso, J. S. Speck, S. Nakamura, and S. P. DenBaars, J. Soc. Inf. Disp. **16**, 571 (2008).
[17]D. F. Feezell, M. C. Schmidt, S. P. DenBaars, and S. Nakamura, MRS Bull. **34**, 318 (2009).
[18]J. E. Northrup, Appl. Phys. Lett. **95**, 133107 (2009).
[19]K. Kojima, M. Funato, Y. Kawakami, S. Masui, S. Nagahama, and T. Mukai, Appl. Phys. Lett. **91**, 251107 (2007).
[20]A. A. Yamaguchi, Jpn. J. Appl. Phys., Part 2 **46**, L789 (2007).
[21]A. Tyagi, H. Zhong, N. N. Fellows, M. Iza, J. S. Speck, S. P. DenBaars, and S. Nakamura, Jpn. J. Appl. Phys., Part 2 **46**, L129 (2007).
[22]K. Kojima, H. Kamon, M. Funato, and Y. Kawakami, Phys. Status Solidi C **5**, 3038 (2008).
[23]S. Khatsevich and D. H. Rich, J. Phys.: Condens. Matter **20**, 215223 (2008).
[24]H. Sato, R. B. Chung, H. Hirasawa, N. Fellows, H. Masui, F. Wu, M. Saito, K. Fujito, J. S. Speck, S. P. DenBaars *et al.*, Appl. Phys. Lett. **92**, 221110 (2008).
[25]M. Ueda, M. Funato, K. Kojima, Y. Kawakami, Y. Narukawa, and T. Mukai, Phys. Rev. B **78**, 233303 (2008).
[26]T. Guhne, Z. Bougrioua, S. Laugt, M. Nemoz, P. Vennegues, B. Vinter, and M. Leroux, Phys. Rev. B **77**, 075308 (2008).
[27]W. G. Scheibenzuber, U. T. Schwarz, R. G. Veprek, B. Witzigmann, and A. Hangleiter, Phys. Rev. B **80**, 115320 (2009).
[28]Y.-R. Wu, Y.-Y. Lin, H.-H. Huang, and J. Singh, J. Appl. Phys. **105**, 013117 (2009).
[29]Y.-R. Wu, C. Chiu, C.-Y. Chang, P. Yu, and H.-C. Kuo, IEEE J. Sel. Top. Quantum Electron. **15**, 1226 (2009).
[30]S. Ghosh, P. Waltereit, O. Brandt, H. T. Grahn, and K. H. Ploog, Phys. Rev. B **65**, 075202 (2002).
[31]H. Masui, H. Asamizu, A. Tyagi, N. F. DeMille, S. Nakamura, and S. P. DenBaars, Appl. Phys. Express **2**, 071002 (2009).
[32]A. Tyagi, Y. D. Lin, D. A. Cohen, M. Saito, K. Fujito, J. S. Speck, S. P. DenBaars, and S. Nakamura, Appl. Phys. Express **1**, 091103 (2008).
[33]H. Sato, A. Tyagi, H. Zhong, N. Fellows, R. B. Chung, M. Saito, K. Fujito, J. S. Speck, S. P. DenBaars, and S. Nakamura, Phys. Status Solidi (RRL) **1**, 162 (2007).
[34]Q. Yan, P. Rinke, M. Scheffler, and C. G. V. de Walle, Appl. Phys. Lett. **95**, 121111 (2009).
[35]S. H. Park, D. Ahn, and S. L. Chuang, IEEE J. Quantum Electron. **43**, 1175 (2007).
[36]I. Vurgaftman and J. R. Meyer, J. Appl. Phys. **94**, 3675 (2003).